Robo signaling regulates the production of cranial neural crest cells

Yan Li[12#], Xiao-tan Zhang[1#], Xiao-yu Wang[1], Guang Wang[1], Manli Chuai[3], Andrea Münsterberg[4], Xuesong Yang[1]*

[1]Division of Histology & Embryology, Key Laboratory for Regenerative Medicine of the Ministry of Education, Medical College, Jinan University, Guangzhou 510632, China

[2] The key Laboratory of Assisted Circulation, Ministry of Health, The First Affiliated Hospital of Sun Yat-sen University, Sun Yat-Sen University,Guangzhou, 510080, China

[3]Division of Cell and Developmental Biology, University of Dundee, Dundee, DD1 5EH, UK

[4]School of Biological Sciences, University of East Anglia, Norwich NR4 7TJ, UK

[#]Contributed to this work equally

[*]Corresponding author: Xuesong Yang (yang_xuesong@126.com) Tel: +86(20)85228316

Abstract

Slit/Robo signaling plays an important role in the guidance of developing neurons in developing embryos. However, it remains obscure whether and how Slit/Robo signaling is involved in the production of cranial neural crest cells. In this study, we examined Robo1 deficient mice to reveal developmental defects of mouse cranial

frontal and parietal bones, which are derivatives of cranial neural crest cells. Therefore, we determined the production of $HNK1^+$ cranial neural crest cells in early chick embryo development after knock-down (KD) of Robo1 expression. Detection of markers for pre-migratory and migratory neural crest cells, PAX7 and AP-2α, showed that production of both was affected by Robo1 KD. In addition, we found that the transcription factor slug is responsible for the aberrant delamination/EMT of cranial neural crest cells induced by Robo1 KD, which also led to elevated expression of E- and N-Cadherin. N-Cadherin expression was enhanced when blocking FGF signaling with dominant-negative FGFR1 in half of the neural tube. Taken together, we show that Slit/Robo signaling influences the delamination/EMT of cranial neural crest cells, which is required for cranial bone development.

Key words: cranial neural crest； Slit/Robo；EMT；delamination；intramembranous ossification

Introduction

In both invertebrate and vertebrate development Slit/Robo signaling exerts a fundamental role in axon guidance at the midline of the central nervous system through repulsing axons away from the midline[1,2]. Slit was initially identified in the *Drosophila* central nervous system as a secreted protein which modulates the growth and migration of glia cells[3]. The mammalian Slit family is composed of three members, Slit1, Slit2 and Slit3, which are expressed in the neural tube during neurulation. Slit1 is principally expressed in the nervous system, and Slit2 and Slit3 are also present in tissues outside of the nervous system[4,5]. The receptors for Slit/ Robo transmembrane proteins, including Robo1, Robo2, Robo3/RIG-1 and Robo4, are predominately expressed on axon growth cones in the central nervous system[6,7]. In addition to its role in neuron development, Slit/Robo signaling also functions in the development of the lung, kidney, heart, muscle and reproductive system[8-11]. Furthermore, Slit/Robo has been implicated in a variety of pathological conditions, such as cancer and inflammation[12,13]. The role of Slit/Robo signaling in the

regulation of cranial neural crest cell (cNCC) production remains poorly understood, although there have been reports on Slit/Robo dependent interactions of cNCC with ectodermal placodes during cranial ganglia formation [14-16]. Many investigations have focused on Slit/Robo functions in trunk neural crest[17-19]. In this study, we address the function of Slit/Robo signaling during cranial neural crest production since cNCC generation is different from that of trunk NCC.

Neural crest cells (NCCs) derive from the dorsal side of the neural tube during early embryo development. NCCs are a population of multipotent cells, which undergo the process of induction, delamination, epithelial-mesenchymal transition (EMT), migration, and eventually give rise to cellular components in almost every organ system in vertebrates[20]. The induction of neural crest at the border of the neural plate relies on signaling molecules from the surrounding neuroepithelium, neural plate and underlying mesoderm [21,22]. The signaling molecules produced by these tissues include bone morphogenetic proteins (BMPs), Wnts, fibroblast growth factors (FGFs) and retinoic acid (RA)[23,24]. An initial BMP gradient activity specifies the neural crest cells at the border of neural plate. The concerted action of Wnt proteins, fibroblast growth factors (FGFs) and retinoic acid (RA) then convert the cells of neural plate border into neural crest cells[25,26]. EMT in neural crest cells is modulated by a number of transcription factor families, including slug, sox, and endothelins (Ets) gene families. These transcription factors regulate cell–cell and cell–matrix adhesion and the detachment of neural crest cells from the neuroepithelium[14].

Massive delamination from the neuroepithelium is characteristic for cranial neural crest cells[27], however the timing for cranial neural crest production varies between chick, mouse and Xenopus[28]. In chick embryos, NCC delaminate concomitantly with the fusion of the neural folds, whereas in mouse and Xenopus NCC depart when the neural plate is still open[29,30]. P53 is a crucial factor controlling the timing of delamination/EMT of cephalic neural crest cells by repressing the transcription factors, slug and Ets1, which then promotes EMT[31]. The regulation of delamination of cNCC is governed by different mechanisms, in part

due to specific morphological characteristics: cNCC are not adjacent to somitic mesoderm as trunk NCC are, instead they receive signals from cranial mesenchyme. Cranial neural crest cells (cNCC) contribute to craniofacial skeleton, cranial ganglia of the sensory nervous system, enteric nervous system, Schwann cells, the wall of the aorta and cardiac septa[32,33]. The abnormal development of neural crest can result in congenital malformations, such as neural tube defects (NTD), atrioventricular septal defects, persistent ductus arteriosus and Waardenburg syndrome[34,35].

Slit/Robo signaling has been shown to be involved in the guidance of cranial neural crest cell migration. For example, Slit/Robo signaling is indispensable for organizing neural crest cells and placode-derived neurons to form the trigeminal ganglion [16]. Slit/Robo signaling is also involved in preventing neuronal and glial neural crest cells from entering the dorsolateral route and the gut[19,17]. However, our experimental data indicated that Slit/Robo signaling might be involved in regulating earlier events during cNCC production. In this study, we employed *Robo1*$^{+/-}$*Robo2*$^{+/-}$ double-heterozygous mice (*Robo1/2*$^{+/-}$) and combined this with Robo1 gain-of-function approaches in early chick embryos to investigate the molecular mechanism of cNCC production.

Materials and Methods

Mouse experiments and alizarin red s staining of whole embryos

Robo1$^{+/-}$ *Robo2*$^{+/-}$ double-heterozygous mice were purchased from MMRRC/ University of Missouri. They were crossed to obtain *Robo1*$^{+/+}$ *Robo2*$^{+/+}$wild-type and *Robo1*$^{+/-}$ *Robo2*$^{+/-}$ double-heterozygous controls, as well as *Robo1*$^{-/-}$ *Robo2*$^{-/-}$ double-knock-out embryos, which were analyzed at E15.5.

To visualize the vertebrate skeleton, the 15.5-day mouse embryos were stained with alizarin red dyes as previously described[36]. Briefly, embryos were fixed in 95% ethanol for 3 days, skin and viscera were carefully removed and embryos were post-fixed for 1 week. Next, embryos were stained in 0.1% alizarin red (Solarbio, Beijing, China) dyes in 70% ethanol for 1 week and then cleared in 25% glycerol/1% KOH for 3 days. Finally, embryos were treated in a graded series of glycerol. The

skeletons were dissected and photographed using a stereomicroscope (Olympus MVX10, Japan). For each genotype replicates of at least 6 embryos were examined and 6 sections were counted for each embryo. All animal experiments were performed according to relevant national and international guidelines and approved by the Medical Research Animal Ethics Committee of Jinan University.

Chick embryos and gene transfection

Fertilized leghorn eggs were acquired from the Avian Farm of South China Agriculture University. They were incubated in a humidified incubator (Yiheng Instruments, Shanghai, China) set at 38^{o}C with 70% humidity. The eggs were incubated until *chick* embryos reached the desired developmental stage (according to Hamburger and Hamilton 1992).

Empty vector pMES was generously supplied by Catherine Krull. The shRNA-Robo1, used for silencing Robo1 expression, was purchased from Open Biosystems. FL-Robo1, a full length rat Robo1 cDNA ligated into pMES, was used for over-expressing Robo1 expression. HH3 (Hamburger and Hamilton stage 3)[37] *chick* embryos were prepared for early *chick* culture, according to methods previously described[38]. The embryos were transfected with plasmid vectors encoding Control-*GFP*, *shRAN-Robo1-GFP* or *PMES-Robo1-GFP* gene by electroporation. Briefly, 0.5 μl plasmid DNA (1.5 mg/ml) was microinjected into the space between the vitelline membrane and the epiblast of *chick* embryos during gastrulation. The electroporation parameters used were as previously described[39]. For one-sided gene transfection, the polarity of the pulses was kept constant. After electroporation, the embryos were incubated for 30 hours. The embryos were photographed and fixed for immunofluorescent staining and *in situ* hybridization. All experiments were performed in replicates of at least 14 embryos.

Immunostaining

Immunofluorescent staining was performed on whole-mount embryos using HNK1, PAX7, AP-2α, E-Cadherin and N-Cadherin antibodies, as previously

described [40,41]. Briefly, embryos were fixed in 4% paraformaldehyde (PFA) at 4^{o}C overnight and then washed with PBS. Unspecific immunoreactions were blocked using 2% Bovine Serum Albumin (BSA) + 1% Triton-X + 1% Tween 20 in PBS for 2 hours at room temperature. The embryos were washed in PBS and incubated with primary monoclonal antibody raised against PAX7 (1:100, DSHB), N-Cadherin (1:100, 6B3, DSHB), HNK1 (1:200, Sigma) and E-Cadherin (1:100, BD), overnight at 4^{o}C on a shaker. Following extensive washing, the embryos were incubated in goat anti-mouse IgG secondary antibody conjugated to Alexa Fluor 555 (1:1000, Invitrogen) overnight at 4^{o}C. All embryos were counterstained with DAPI (4'-6-Diamidino-2-phenylindole, 1:1000, Invitrogen) for 30 min at room temperature. All immunofluorescent staining was performed in replicates of at least 6 embryos.

After immunofluorescent staining, the whole-mount embryos were photographed by using a stereo-fluorescence microscope (Olympus MVX10; OLYMPUS, Tokyo, Japan) and processed with Olympus software package Image-Pro Plus 7.0. Then, the embryos were sectioned into 15-μm thick slices by using a cryostat microtome (Leica CM1900; LEICA, Solms, Germany) and photographed by using an epi-fluorescent microscope (Olympus IX51, Leica DM 4000B) at a magnification of 200 × or 400 ×. The images were analyzed and processed by using a CW4000 FISH Olympus software package.

In situ hybridization

Whole-mount in situ hybridization of *chick* embryos was performed according to previously described protocols[42]. Digoxigenin-labeled antisense RNA probes were synthesized against *Slug*[43]. The whole-mount stained embryos were photographed and 15 μm sections were prepared on a cryostat microtome (Leica CM1900).

RNA isolation and RT-PCR

Total RNA was isolated from embryonic cranial tissues using Trizol kit (Invitrogen, USA) according to the manufacturer's instructions. First-strand cDNA was synthesized in a final volume of 25μl using SuperScript Ⅲ First-Strand

(Invitrogen, USA). Following reverse transcription, PCR amplification was performed using specific primers for *chick PAX7* (5'-GCTTACTGAAGAGGTCCGACTGTG-3' and 5'-ACAAGTTGATGCGAGGTGGAAGG-3'), *slug* (5'-CTGCCTTCAAAATGCCAC-3' and *5*'-TCTCTCTTAGGTCAGGTT-3' ）， *E-Cadherin* (*5*'-CGCTTCCCCGTGTTGGT-3' and 5'-GGCCGTTTTGTTGAGACGAC-3' 60°C*),* *Robo1* (5'-AAGCACCAAAACGAGAAGGC-3' and 5'-TCTCCCTCCTGATCCTCTCG-3') and *GAPDH* (5'-GAGAACGGGAAACTTGTCAT-3' and 5'-GGCAGGTCAGGTCAACAA-3'*)*. PCR was performed in a Bio-Rad S1000^{TM} Thermal cycler (Bio-Rad, USA). cDNAs were amplified for 30 cycles. One round of amplification was performed at 98°C for 10 sec, at 60°C for 15 sec and at 72°C for 30 sec (TaKaRa, Japan). The PCR products (20 μl) were resolved on 1% agarose gels (Biowest, Spain) in 1× TAE buffer (0.04 M Tris-acetate and 0.001 M EDTA), and GeneGreen Nucleic Acid Dye (TIANGEN, China). Reaction products were visualized using a trans illuminator (SYNGENE, UK) and a computer-assisted gel documentation system (SYNGENE).

Data analysis

We define the phenotypes of inhibition, no effect, and promotion mainly based on the analysis of sections from per embryo. Immunofluorescent staining was quantified from at least five sections which are at midbrain level per embryo, and five embryos were at least chosen from per group. Sections were randomly selected and analyzed under blinded conditions. All immunofluorescent analyses were repeated at least three times and the representative images were presented eventually.

A minimum of four experimental animals and controls were evaluated in all experiments. Data analyses and construction of statistical charts were performed using Graphpad Prism 5 software (Graphpad Software, CA, USA). Results were presented as mean value ($\bar{x}$±SE). The data of frequency was analyzed using nonparametric tests，the other data were analyzed using ANOVA, which was employed to establish whether there was any difference between control and experimental data. *P<0.05,

**P<0.01 and ***P<0.001 indicate significant difference between experimental and control embryos.

Results

Development of the mouse craniofacial skeleton is affected in absence of Robo1

To determine the role of Robo1 and Robo2 for the formation of the craniofacial skeleton, we used an available strain of Robo1/2 knock-out mice. We found that E15.5 double-knock-out *Robo1*$^{-/-}$*; Robo2*$^{-/-}$ mice were smaller (11.34±0.11 mm, N=12, P<0. 05) compared to E15.5 wild type (*Robo1*$^{+/+}$ *Robo2*$^{+/+}$) (12.03±0.13 mm, N=12) or double-heterozygous (*Robo1*$^{+/-}$ *Robo2*$^{+/-}$) (11.91±0.12 mm, N=12) mice (Fig. 1a-d). In addition, double-knock-out *Robo1*$^{-/-}$; *Robo2*$^{-/-}$ mice exhibited internal hemorrhaging. Alizarin Red staining of E15.5 mouse embryonic heads revealed a defect in parietal and frontal bone development (Fig. 1e'-g' arrows) in 66.7% (Fig. 1h) of *Robo1*$^{-/-}$; *Robo2*$^{-/-}$ mice in comparison to wild-type *Robo1*$^{+/+}$; *Robo2*$^{+/+}$ mice. There was no apparent defect observed in *Robo1*$^{+/-}$; *Robo2*$^{+/-}$ double-heterozygous mice. These data suggest that loss of *Robo1/2* during development led to defects in the craniofacial skeleton.

In addition, we used function blocking R5 antibody to suppress Slit/Robo signaling[34]. After injection of R5 antibody into neural tubes of HH10 chick embryos, and incubation until E15, the treated embryos were smaller and had defects in parietal and frontal bone development in comparison to control embryos (Fig. S1). The phenotypes observed were quantified (Fig. S1e) and the majority of embryos showed the effect.

Manipulation of Robo1 expression levels in chick embryos altered the generation of cranial neural crest cells

Cranial neural crest cells (cNCC) gives rise to cartilage and bone of the face and skull[44]. To determine the developmental origin of the defects observed in parietal and frontal bones of *Robo1-/-*; *Robo2-/-* double-knock-out mice, we examined the function of Robo1 in the early stage of neural crest generation. Both knock-down and

over-expression experiments were performed in chick embryos. Plasmids encoding either shRNA-Robo1-GFP or PMES-Robo1 were transfected into half of the neural plate at HH3. Embryos were further incubated for 30 hours. RT-PCR analysis showed that Robo1 was expressed in cranial and trunk neural tubes of HH10 chick embryos (Fig. 2a), and Robo1 expression was slightly decreased after shRNA-Robo1-GFP transfection and slightly increased after PMES-Robo1 transfection in chick neural tube (Fig. 2b). Cranial migratory neural crest cells were detected by whole-mount HNK1 immunofluorescent staining[45]. Control embryos were transfected with empty vector, Control-GFP (Fig. 2c-e). Whole mount embryos (Fig. 2d) and sections (Fig. 2e-e") illustrate that gene transfection was successful and the procedure itself did not affect $HNK1^+$ cranial neural crest cell production (Fig. 2c-e, l). However, after Robo1 knock-down using shRNA-Robo1-GFP transfection the production of $HNK1^+$ cranial neural crest cells was inhibited in 68.6% of embryos as shown in whole mount and in sections, compared to 19.05% in Control-GFP group (n= 24/35, $P<0.001$) (Fig. 2f-h, l). Targeted over-expression of Robo1 using transfection of PMES-Robo1-GFP promoted the production of $HNK1^+$ cranial neural crest cells (n=12/21, $P<0.01$) (Fig. 2i-k, l). Higher magnifications of transverse sections allow comparisons between the transfected and control sides of embryos (Fig. 2e-e", h-h", k-k") and counting of $HNK1^+$ cells. Also, there were significantly less $HNK\text{-}1^+$ cells in the shRNA-Robo1-GFP embryos (17.97±1.60%, n=8, $P<0.001$), while significantly more $HNK\text{-}1^+$ cells were presented in the PMES-Robo1 embryos (62.32±2.48%, n=7, $P<0.01$) compared to control (52.12±0.86%, n=8, Fig. 2m). Taken together, manipulation of Robo1 function *in vivo* implicates Slit2/Robo1 signaling in the regulation of cranial neural crest cell production.

Next, we determined the production of $PAX7^+$ cranial neural crest cells after Robo1 gain- or loss-of-function using transfection of either shRNA-Robo1 or PMES-Robo1 in neural tubes of HH10 chick embryos (Fig. 2). PAX7 is expressed in pre-migratory (dorsal neural tube) and migratory neural crest cells during neurulation[46,47]. Transfection of Control-GFP had no effect on production of $PAX7^+$ cranial neural crest cells, which are shown in whole mount embryos and

transverse sections (Fig. 2n, n'). However, 50% of embryos after shRNA-Robo1 transfected in neural tube restricted the production of $PAX7^+$ cranial neural crest cells (n=9/18, P<0.05) (Fig. 2o, o', q), while elevated Robo1 expression promoted the production of $PAX7^+$ cranial neural crest cells in 71.43% of embryos after PMES-Robo1 transfection (n=10/14, P<0.01) (Fig. 2p, p', q). We quantified the results obtained by counting the number of GFP^+ and $PAX7^+$ cells in transverse sections of transfected embryos (Fig. 2n', o' p'). This showed a decrease in $GFP^+/PAX7^+$ cells（54.54±1.71%, n=5）following Robo1 KD (29.66±4.08%, n=5, P<0.01) and an increase following Robo1 over-expression (68.12±3.63%, n=5, P<0.01, Fig. 2r). RT-PCR data demonstrated reduced levels of PAX7 transcripts after KD and increased levels of PAX7 transcripts in dissected dorsal neural tubes (Fig. 2s). This was consistent with PAX7 immunostaining and confirmed observations of HNK1 staining of cranial neural tubes.

Robo1 KD resulted in down-regulation of slug expression in chick neural tube.

Pre-migratory neural crest cells undergo epithelial-to-mesenchymal transition (EMT) to become migratory and to emerge from the dorsal neural tube[48]. The transcription factor, Slug, can induce EMT in neural epithelial cells[49]. Therefore, we examined if Slug expression was affected by Robo1 KD in developing neural tubes (Fig. 3). GFP expression indicates successful transfection and merged images of Control-GFP or shRNA-Robo1 (Fig.3b, f) with slug *in situ* hybridization are shown (Fig. 3a, e). To confirm the negative effect of Robo1 KD on cNCC production, we carried out HNK1 immunostaining in the same transfected embryos (Fig. 3c-d, g-h). The number of $HNK1^+$ cNCCs was reduced as before. The quantitative analysis of the observed phenotypes is shown in Fig. 3i (n=28/36, P<0.01). RT-PCR data showed that slug gene expression in the dissected dorsal/cranial neural tube was reduced following transfection of shRNA-Robo1 (Fig. 3j). The results suggest that inhibitory effects on migratory cNCC and EMT might be due to reduced slug expression induced by Robo1 KD in neural tubes.

Robo1 KD promoted expression of adhesion molecules in chick neural tube.

During EMT, epithelial cells lose their cell-cell adhesion and acquire individual migratory properties. Thus, we next determined whether reduced slug expression after Robo1 KD correlated with a change in expression of adhesion molecules. E-Cadherin was expressed in the neural tube of HH9 embryos (Fig. 4a, c), the cranial neural tube and neural crest in embryos transfected with Control-GFP or shRNA-Robo1 (Fig. 4a-a’’’, b-b’’’, c-c’’) and transfection of Control-GFP had no effect on production of $HNK1^+$ cranial neural crest cells, which are shown in whole mount embryos and transverse sections (Fig. 4a-a’’’, d). However, Robo1 KD in neural tube increased the expression of E-Cadherin in a majority of embryos (n=15/22, P<0.001) (Fig. 4b-b’’’, c-c’’’, d). RT-PCR showed that E-Cadherin expression was enhanced after shRNA-Robo1 transfection in chick cranial neural tube (Fig. 4e).

Next, we detected the expression of N-Cadherin following the transfection of shRNA-Robo1 into one half of the neural tube (Fig. 5c-d). In comparison to Control-GFP control (Fig. 5a-b), N-Cadherin expression was enhanced in the shRNA-Robo1 transfected side of the neural tube and migrating NCCs (Fig. 5c-d). The numbers of different phenotype are shown in Fig. 5h (n=15/19, P<0.001). To confirm the importance of N-Cadherin expression for neural crest EMT we determined the effect of manipulating N-Cadherin expression on cranial neural crest production. We transfected either wild-type N-Cadherin (Wt-N-Cad) (Fig. 5f-f”) or dominant negative N-Cadherin (Dn-N-Cad) (Fig. 5g-g”) into one half of the neural tube, Control-GFP transfection served as control (Fig. 5e-e’’). Over-expression of wt-N-Cad resulted in reduced production of $HNK1^+$ cNCCs compared to the control side (n=12/18, P<0.01) (Fig. 5f-f”, i), whilst Dn-N-Cad transfection led to enhanced $HNK1^+$ cNCC production (n=15/24, P<0.01) (Fig. 5g-g”, i).

Next, we determined whether the effect of Robo1 KD could be reversed by co-transfecting Robo1-shRNA-GFP with Dn-N-Cad-GFP into one side of the neural tube. HNK1 expression was restored to normal in these embryos (Fig. 6d-f). Co-transfection of Control-GFP-GFP with Dn-N-Cad-GFP served as control (Fig. 6a-c) and the phenotype of these embryos was similar to those transfected with

Dn-N-Cad-GFP alone (Fig. 5g-g”). The phenotypes observed were quantified (Fig. 6g) and in a majority of embryos cNCC production was rescued (n=12/22, P<0.01). The data indicate that the Robo1-shRNA-induced phenotype - reduced $HNK1^+$ cNCC production, was rescued by interfering with N-Cadherin function suggesting Robo1 may negatively regulate N-Cadherin expression.

FGF signaling regulates N-cadherin mediated EMT during cNCC production

FGF signaling has been shown to affect production of trunk NCCs through regulating EMT[50,51]. To investigate whether disruption of FGF signaling can affect expression of N-Cadherin in cranial neural tube, we transfected dominant negative FGFR1 (Dn-FGFR1) (Fig. 7b-b’’). The empty vector, Control-GFP, served as transfection control (Fig. 7a-a’’). N-Cadherin immunostaining showed that Control-GFP transfection did not affect its expression in neural tube (Fig. 7a’-a”). In contrast, blocking FGF signaling with Dn-FGFR1 transfection increased N-Cadherin expression in transfected neural tube compared to control side (n=17/24, P<0.001) (Fig. 7b’-b”,g). Furthermore, fewer $PAX7^+$ migratory cNCCs were observed on the Dn-FGFR1-GFP transfected side of the cranial neural tube (25.68±0.90%, n=6, P<0.001, Fig. 7d’-d’’, f’-f”) compared to control neural tubes (55.89±1.90%, n=6, Fig. 7d’-d”, e’-e’’, h). The empty vector, Control-GFP, serves as transfection control (Fig. 7c-c’’). This shows that FGFR signaling is required for the production of cranial NCC and indicates a possible interaction of FGF and Robo1 during cNCC production.

Discussion

Although there are differences between cranial and trunk neural crest production, both of these populations are determined by a combination of intrinsic and extrinsic factors. Intrinsic factors include genetic networks and extrinsic factors define the microenvironment during neural crest induction, delamination and migration. Therefore, understanding how these factors are involved in regulating the delamination/EMT and migration of NCCs is essential to comprehend the mechanism of their production[15].

In HH4 chick embryos, Slit is expressed in the Hensne's node, and it appears in the prechordal plate, the notochord, and the somites at HH8 stage of chick embryo. In HH 10 stage of chick embryo, Slit expresses in the prechordal plate, the floor plate (FP), the roof plate (RP) and notochord, as well as in the early neural tube and muscle [14]. Robo1, the Slit receptor, is also expressed in the developing neural tube and proximal somites in the early stages of chick embryo development [15,16]. The neural crest cells delaminate at the edge of the neural plate, where there is not expression of Slit/Robo in vertebrates. In this study, we reveal that Slit/Robo signaling influences on the delamination/EMT of neural crest, which extends an earlier regulative role of Robo1 in the development of neural crest cells.

As we know，many adverse nutritional or environmental factors that occur during critical periods of fetal development may have a permanent effect on organ morphology, metabolism and function at the time of adulthood[9,10]. And Slit-Robo signaling is deemed to be involved in the regulation of cell migration, cell death and angiogenesis and so on. Mathilda T.M. et al. have demonstrated the Robo signal also played an important role during embryonic cardiogenesis. Their study reveals that the embryos without robo1 displayed the lack part of the pericardium and systemic venous return defects. In addition, the reduction of the Slit3 protein in the absence of Robo1, resulting in damaged heart neural crest, adhesion and migration, is the basis of cardiac defects[11]. Slit-Robo signaling plays important roles in the axon guidance, axon branching, neuronal migration and morphological differentiation. Furthermore, SRGAP genes, originally identified as a downstream mediator of Slit and Robo receptor, may be linked to some neurodevelopmental disorders such as mental retardation, schizophrenia and so on [12]. Volker Endris et al. have confirmed that the lack of MEGAP srGAP3, the direct intracellular portion of this signal transduction pathway, may inhibit the normal migration of neural progenitor cells to their ultimate location in the nervous system[13]. In summary, dysfunction of Slit-Robo signaling contributes to the congenital cardiac and nervous system diseases.

Osteogenesis in the vertebrate skull is achieved through intramembranous ossification of mesenchymal cNCCs[44]. In order to investigate whether Robo

signaling is involved in this process, we analyzed phenotypes of Robo1 and Robo2 double knock-out mice. This revealed that Robo1/2 double knock-out mice were smaller, had internal hemorrhaging and, importantly, abnormal development of frontal and parietal bones (Fig. 1), which are neural crest-derived and mesoderm-derived respectively. In addition, most craniofacial bones come from cranial neural crest cells[32,44], which thus contribute to the developing face. Therefore, the potential involvement of Robo signaling in the production of cNCCs, which is a prerequisite for the formation of intramembranous bones, was investigated in early stage *chick* embryos. These are readily accessible and allow the spatiotemporal manipulation of gene expression. Targeted mis-expression or knock-down (KD) of Robo1 was achieved during cNCC production (Fig. 2). Using markers for pre-migratory (PAX7) and migratory NCCs (HNK1), we showed that KD of Robo1 expression mediated by shRNA-Robo1 significantly inhibited cNCC production on the transfected side of the neural tube (Fig. 2). In contrast, up-regulation of Robo1 expression by transfection of PMES-Robo1 increased cNCC production based on immunostaining with HNK1 and PAX7. Thus, Robo signaling is important during both pre-migratory and migratory cNCC production. This could be for multiple reasons such as effects on proliferation/apoptosis of NCCs. In this study, we focused on potential defects during neural crest delamination/EMT.

The transcription factor, Slug, plays a vital role in NCC delamination/EMT through modulating the expression of adhesion molecules[31]. For example, cadherin6B is directly suppressed by Slug during EMT of the neural crest[52]. Here, we chose HH9 and HH11, which are the most active periods for cNCC delamination/EMT. Slug expression was repressed by Robo1 KD at both time points, shown by transverse sections (Fig. 3). This correlated with fewer $HNK1^{+}$ cells and enhanced expression of N-Cadherin (Figs. 3 and 4). Neural crest cell specification at the neural plate border is regulated by a series of inductive signals and transcription factors[21,22]. After they are specified, neural crest cell undergo an epithelial-to-mesenchymal transition companied by dramatic changes in cell adhesion. Then they emigrate from the neural tube to reach their final destinations in the

embryo[53,54]. Many studies have confirmed that N-cadherin has an essential role in neural cell migration[55,56]. In addition, the crucial role of N-cadherin in cell adhesion and its interaction with Slit1-Robo2 during gangliogenesis was demonstrated in vivo[16]. Our observations regarding the interplay between Robo with N-cadherin during the production of cranial NCCs are consistent with these previous studies. Targeted mis-expression of Wt-N-Cadherin in neural tube led to reduced production of $HNK1^+$ cNCCs, whereas Dn-N-Cadherin transfection had the opposite effect (Fig. 5). Furthermore, the effect of Robo KD was rescued by co-transfection of Dn-N-Cadherin (Fig. 6). Our findings also suggest that reduced Slug expression resulting from Robo1 KD is at least partially responsible for the defect in cNCC delamination/EMT. This is consistent with the known expression patterns of these factors during neural development[57]. We propose that altered Robo signaling affects Slug expression and thus cNCC delamination/EMT, which is achieved via targeting adhesion molecules[31,52].

It was shown previously that FGFR1 plays an important role for the development of cranial neural crest derivatives, and blocking FGF signaling with Dn-FGFR1 in NCCs leads to cleft palate in later stage embryos[58]. FGFR1 mutants affect cranial crest cell differentiation and result in the activation of chondrogenesis. Furthermore, FGFR-mediated signaling is required for EMT of mesoderm cells emerging from the primitive streak during gastrulation[51,39]. We demonstrate here that FGFR1 is also involved in regulating N-Cadherin expression and the production of $PAX7^+$ migratory cNCCs (Fig. 7) consistent with a previous report showing that inhibition of FGF signaling decreased the expression of Pax7[59].

We showed previously that PDGF and FGF signaling influence N-Cadherin expression in migrating mesoderm cells during *chick* gastrulation, enabling them to migrate towards their target destinations[40]. N-Cadherin might play a similar role in cNCCs migration as it does in mesoderm cells of gastrula embryos. Interestingly, Robo signaling has been shown to target E-Cadherin in colorectal cancer cells[60] and an E- to N-Cadherin switch regulates contact inhibition of locomotion migrating neural crest in Xenopus, where these adhesion molecules contribute to redistribution

of forces to the extracellular matrix[61]. Thus, both E- and N-Cadherin are important for the processes of neural crest delamination and migration, and we propose that delamination/EMT of cNCCs depends on the interaction between E-Cadherin to N-Cadherin, which is regulated by Slug in response to Robo1 and FGFR signaling (Fig. 8)[62,63]. At present it is not possible to determine how FGF and Robo1 signaling pathways interact, and further studies will be necessary to investigate whether they are dependent on each other or act in parallel.

Acknowledgements

We would like to thank Prof. Jian-guo Geng for providing shRNA-Robo1-GFP and PMES-Robo1 plasmids. This study was supported by NSFC grant (81571436); National Natural Science Foundation of Guangdong (2016A030311044); Science and Technology Planning Project of Guangdong Province (2014A020213008); Science and Technology Program of Guangzhou (201510010073).

Author contributions

Y.L., X.Z., X.W. and G.W. performed the experiments and collected the date; G.W., M.C. and X.Y. designed the study and analyzed the date; A.M. and X.Y. wrote manuscript.

Compliance with Ethical Standards

Competing financial interest

The authors declare that they have no conflict of interest.

References

1. Dickson BJ (2002) Molecular mechanisms of axon guidance. Science 298 (5600):1959-1964. doi:10.1126/science.1072165

2. Dickson BJ, Gilestro GF (2006) Regulation of commissural axon pathfinding by slit and its Robo receptors. Annu Rev Cell Dev Biol 22:651-675. doi:10.1146/annurev.cellbio.21.090704.151234

3. Rothberg JM, Hartley DA, Walther Z, Artavanis-Tsakonas S (1988) slit: an EGF-homologous locus of D. melanogaster involved in the development of the embryonic central nervous system. Cell 55 (6):1047-1059
4. Yuan W, Zhou L, Chen JH, Wu JY, Rao Y, Ornitz DM (1999) The mouse SLIT family: secreted ligands for ROBO expressed in patterns that suggest a role in morphogenesis and axon guidance. Developmental biology 212 (2):290-306. doi:10.1006/dbio.1999.9371
5. Piper M, Georgas K, Yamada T, Little M (2000) Expression of the vertebrate Slit gene family and their putative receptors, the Robo genes, in the developing murine kidney. Mech Dev 94 (1-2):213-217
6. Enomoto S, Mitsui K, Kawamura T, Iwanari H, Daigo K, Horiuchi K, Minami T, Kodama T, Hamakubo T (2016) Suppression of Slit2/Robo1 mediated HUVEC migration by Robo4. Biochemical and biophysical research communications 469 (4):797-802. doi:10.1016/j.bbrc.2015.12.075
7. Enomoto S, Mitsui K, Kawamura T, Iwanari H, Daigo K, Horiuchi K, Minami T, Kodama T, Hamakubo T (2016) Suppression of Slit2/Robo1 mediated HUVEC migration by Robo4. Biochem Bioph Res Co 469 (4):797-802
8. Harpaz N, Ordan E, Ocorr K, Bodmer R, Volk T (2013) Multiplexin promotes heart but not aorta morphogenesis by polarized enhancement of slit/robo activity at the heart lumen. PLoS genetics 9 (6):e1003597. doi:10.1371/journal.pgen.1003597
9. Dickinson RE, Duncan WC The SLIT-ROBO pathway: a regulator of cell function with implications for the reproductive system. Reproduction 139 (4):697-704
10. Fish JE, Wythe JD, Xiao T, Bruneau BG, Stainier DY, Srivastava D, Woo S (2011) A Slit/miR-218/Robo regulatory loop is required during heart tube formation in zebrafish. Development 138 (7):1409-1419. doi:10.1242/dev.060046
11. Ordan E, Volk T (2015) Cleaved Slit directs embryonic muscles. Fly (Austin) 9 (2):82-85. doi:10.1080/19336934.2015.1102808
12. Hinck L (2004) The versatile roles of "axon guidance" cues in tissue morphogenesis. Dev Cell 7 (6):783-793. doi:10.1016/j.devcel.2004.11.002
13. Chedotal A, Kerjan G, Moreau-Fauvarque C (2005) The brain within the tumor: new roles for axon guidance molecules in cancers. Cell Death Differ 12 (8):1044-1056. doi:10.1038/sj.cdd.4401707
14. Theveneau E, Mayor R Neural crest migration: interplay between chemorepellents, chemoattractants, contact inhibition, epithelial-mesenchymal transition, and collective cell migration. Wiley interdisciplinary reviews 1 (3):435-445
15. Kuriyama S, Mayor R (2008) Molecular analysis of neural crest migration. Philos Trans R Soc Lond B Biol Sci 363 (1495):1349-1362. doi:10.1098/rstb.2007.2252
16. Shiau CE, Bronner-Fraser M (2009) N-cadherin acts in concert with Slit1-Robo2 signaling in regulating aggregation of placode-derived cranial sensory neurons. Development 136 (24):4155-4164. doi:10.1242/dev.034355
17. Jia L, Cheng L, Raper J (2005) Slit/Robo signaling is necessary to confine early neural crest cells to the ventral migratory pathway in the trunk. Developmental biology 282 (2):411-421. doi:10.1016/j.ydbio.2005.03.021
18. Wang G, Li Y, Wang XY, Han Z, Chuai M, Wang LJ, Ho Lee KK, Geng JG, Yang X Slit/Robo1 signaling regulates neural tube development by balancing neuroepithelial cell proliferation and differentiation. Experimental cell research 319 (8):1083-1093
19. De Bellard ME, Rao Y, Bronner-Fraser M (2003) Dual function of Slit2 in repulsion and enhanced migration of trunk, but not vagal, neural crest cells. The Journal of cell biology 162 (2):269-279.

doi:10.1083/jcb.200301041
20. Hall BK (2008) The neural crest and neural crest cells: discovery and significance for theories of embryonic organization. J Biosci 33 (5):781-793
21. LaBonne C, Bronner-Fraser M (1998) Neural crest induction in Xenopus: evidence for a two-signal model. Development 125 (13):2403-2414
22. LaBonne C, Bronner-Fraser M (1999) Molecular mechanisms of neural crest formation. Annu Rev Cell Dev Biol 15:81-112. doi:10.1146/annurev.cellbio.15.1.81
23. Anderson MJ, Schimmang T, Lewandoski M (2016) An FGF3-BMP Signaling Axis Regulates Caudal Neural Tube Closure, Neural Crest Specification and Anterior-Posterior Axis Extension. PLoS genetics 12 (5):e1006018. doi:10.1371/journal.pgen.1006018
24. Maj E, Kunneke L, Loresch E, Grund A, Melchert J, Pieler T, Aspelmeier T, Borchers A (2016) Controlled levels of canonical Wnt signaling are required for neural crest migration. Developmental biology 417 (1):77-90. doi:10.1016/j.ydbio.2016.06.022
25. Barembaum M, Bronner-Fraser M (2005) Early steps in neural crest specification. Semin Cell Dev Biol 16 (6):642-646. doi:10.1016/j.semcdb.2005.06.006
26. Steventon B, Carmona-Fontaine C, Mayor R (2005) Genetic network during neural crest induction: from cell specification to cell survival. Semin Cell Dev Biol 16 (6):647-654. doi:10.1016/j.semcdb.2005.06.001
27. Theveneau E, Mayor R Collective cell migration of the cephalic neural crest: the art of integrating information. Genesis 49 (4):164-176
28. Gouignard N, Maccarana M, Strate I, von Stedingk K, Malmstrom A, Pera EM (2016) Musculocontractural Ehlers-Danlos syndrome and neurocristopathies: dermatan sulfate is required for Xenopus neural crest cells to migrate and adhere to fibronectin. Dis Model Mech 9 (6):607-620
29. Jacques-Fricke BT, Roffers-Agarwal J, Gammill LS (2012) DNA Methyltransferase 3b Is Dispensable for Mouse Neural Crest Development. Plos One 7 (10)
30. Theveneau E, Duband JL, Altabef M (2007) Ets-1 confers cranial features on neural crest delamination. Plos One 2 (11):e1142. doi:10.1371/journal.pone.0001142
31. Rinon A, Molchadsky A, Nathan E, Yovel G, Rotter V, Sarig R, Tzahor E p53 coordinates cranial neural crest cell growth and epithelial-mesenchymal transition/delamination processes. Development (Cambridge, England) 138 (9):1827-1838
32. Cordero DR, Brugmann S, Chu Y, Bajpai R, Jame M, Helms JA (2011) Cranial neural crest cells on the move: their roles in craniofacial development. Am J Med Genet A 155A (2):270-279. doi:10.1002/ajmg.a.33702
33. Eames BF, Schneider RA (2008) The genesis of cartilage size and shape during development and evolution. Development 135 (23):3947-3958
34. Wang G, Li Y, Wang XY, Han Z, Chuai M, Wang LJ, Ho Lee KK, Geng JG, Yang X (2013) Slit/Robo1 signaling regulates neural tube development by balancing neuroepithelial cell proliferation and differentiation. Experimental cell research 319 (8):1083-1093. doi:10.1016/j.yexcr.2013.02.011
35. Bergeron KF, Nguyen CM, Cardinal T, Charrier B, Silversides DW, Pilon N (2016) Upregulation of the Nr2f1-A830082K12Rik gene pair in murine neural crest cells results in a complex phenotype reminiscent of Waardenburg syndrome type 4. Dis Model Mech 9 (11):1283-1293. doi:10.1242/dmm.026773
36. Solloway MJ, Dudley AT, Bikoff EK, Lyons KM, Hogan BL, Robertson EJ (1998) Mice lacking Bmp6 function. Dev Genet 22 (4):321-339.

doi:10.1002/(SICI)1520-6408(1998)22:4<321::AID-DVG3>3.0.CO;2-8
37. Hamburger V, Hamilton HL (1992) A series of normal stages in the development of the chick embryo. 1951. Dev Dyn 195 (4):231-272
38. Chapman SC, Collignon J, Schoenwolf GC, Lumsden A (2001) Improved method for chick whole-embryo culture using a filter paper carrier. Dev Dyn 220 (3):284-289. doi:10.1002/1097-0177(20010301)220:3<284::AID-DVDY1102>3.0.CO;2-5
39. Yang X, Dormann D, Munsterberg AE, Weijer CJ (2002) Cell movement patterns during gastrulation in the chick are controlled by positive and negative chemotaxis mediated by FGF4 and FGF8. Dev Cell 3 (3):425-437
40. Yang X, Chrisman H, Weijer CJ (2008) PDGF signalling controls the migration of mesoderm cells during chick gastrulation by regulating N-cadherin expression. Development 135 (21):3521-3530. doi:10.1242/dev.023416
41. Yue Q, Wagstaff L, Yang X, Weijer C, Munsterberg A (2008) Wnt3a-mediated chemorepulsion controls movement patterns of cardiac progenitors and requires RhoA function. Development 135 (6):1029-1037. doi:10.1242/dev.015321
42. Henrique D, Adam J, Myat A, Chitnis A, Lewis J, Ish-Horowicz D (1995) Expression of a Delta homologue in prospective neurons in the chick. Nature 375 (6534):787-790. doi:10.1038/375787a0
43. Leslie NR, Yang X, Downes CP, Weijer CJ (2007) PtdIns(3,4,5)P(3)-dependent and -independent roles for PTEN in the control of cell migration. Curr Biol 17 (2):115-125. doi:10.1016/j.cub.2006.12.026
44. Santagati F, Rijli FM (2003) Cranial neural crest and the building of the vertebrate head. Nat Rev Neurosci 4 (10):806-818. doi:10.1038/nrn1221
45. Li W, Huang L, Lin W, Ke Q, Chen R, Lai X, Wang X, Zhang J, Jiang M, Huang W, Wang T, Yang X, Chen Y, Song W, Xiang AP Engraftable neural crest stem cells derived from cynomolgus monkey embryonic stem cells. Biomaterials 39:75-84
46. Lacosta AM, Canudas J, Gonzalez C, Muniesa P, Sarasa M, Dominguez L (2007) Pax7 identifies neural crest, chromatophore lineages and pigment stem cells during zebrafish development. Int J Dev Biol 51 (4):327-331. doi:10.1387/ijdb.062217al
47. Basch ML, Bronner-Fraser M, Garcia-Castro MI (2006) Specification of the neural crest occurs during gastrulation and requires Pax7. Nature 441 (7090):218-222. doi:10.1038/nature04684
48. Wu CY, Hooper RM, Han K, Taneyhill LA Migratory neural crest cell alphaN-catenin impacts chick trigeminal ganglia formation. Developmental biology 392 (2):295-307
49. Cheung M, Chaboissier MC, Mynett A, Hirst E, Schedl A, Briscoe J (2005) The transcriptional control of trunk neural crest induction, survival, and delamination. Dev Cell 8 (2):179-192. doi:10.1016/j.devcel.2004.12.010
50. Martinez-Morales PL, Diez del Corral R, Olivera-Martinez I, Quiroga AC, Das RM, Barbas JA, Storey KG, Morales AV FGF and retinoic acid activity gradients control the timing of neural crest cell emigration in the trunk. The Journal of cell biology 194 (3):489-503
51. Ciruna B, Rossant J (2001) FGF signaling regulates mesoderm cell fate specification and morphogenetic movement at the primitive streak. Dev Cell 1 (1):37-49
52. Taneyhill LA, Coles EG, Bronner-Fraser M (2007) Snail2 directly represses cadherin6B during epithelial-to-mesenchymal transitions of the neural crest. Development 134 (8):1481-1490. doi:10.1242/dev.02834
53. Carmona-Fontaine C, Matthews HK, Kuriyama S, Moreno M, Dunn GA, Parsons M, Stern CD,

Mayor R (2008) Contact inhibition of locomotion in vivo controls neural crest directional migration. Nature 456 (7224):957-961. doi:10.1038/nature07441
54. Kulesa PM, Fraser SE (2000) In ovo time-lapse analysis of chick hindbrain neural crest cell migration shows cell interactions during migration to the branchial arches. Development 127 (6):1161-1172
55. Bronner-Fraser M, Wolf JJ, Murray BA (1992) Effects of antibodies against N-cadherin and N-CAM on the cranial neural crest and neural tube. Developmental biology 153 (2):291-301
56. Xu X, Li WE, Huang GY, Meyer R, Chen T, Luo Y, Thomas MP, Radice GL, Lo CW (2001) Modulation of mouse neural crest cell motility by N-cadherin and connexin 43 gap junctions. The Journal of cell biology 154 (1):217-230
57. Dady A, Blavet C, Duband JL Timing and kinetics of E- to N-cadherin switch during neurulation in the avian embryo. Developmental dynamics : an official publication of the American Association of Anatomists 241 (8):1333-1349
58. Wang C, Chang JYF, Yang CF, Huang YQ, Liu JC, You P, McKeehan WL, Wang F, Li XK (2013) Type 1 Fibroblast Growth Factor Receptor in Cranial Neural Crest Cell-derived Mesenchyme Is Required for Palatogenesis. J Biol Chem 288 (30):22174-22183
59. Stuhlmiller TJ, Garcia-Castro MI (2012) FGF/MAPK signaling is required in the gastrula epiblast for avian neural crest induction. Development 139 (2):289-300
60. Zhou WJ, Geng ZH, Chi S, Zhang W, Niu XF, Lan SJ, Ma L, Yang X, Wang LJ, Ding YQ, Geng JG Slit-Robo signaling induces malignant transformation through Hakai-mediated E-cadherin degradation during colorectal epithelial cell carcinogenesis. Cell research 21 (4):609-626
61. Scarpa E, Szabo A, Bibonne A, Theveneau E, Parsons M, Mayor R (2015) Cadherin Switch during EMT in Neural Crest Cells Leads to Contact Inhibition of Locomotion via Repolarization of Forces. Dev Cell 34 (4):421-434. doi:10.1016/j.devcel.2015.06.012
62. Luo Y, High FA, Epstein JA, Radice GL (2006) N-cadherin is required for neural crest remodeling of the cardiac outflow tract. Developmental biology 299 (2):517-528
63. Rogers CD, Saxena A, Bronner ME (2013) Sip1 mediates an E-cadherin-to-N-cadherin switch during cranial neural crest EMT. The Journal of cell biology 203 (5):835-847. doi:10.1083/jcb.201305050

Figure and Figure legends

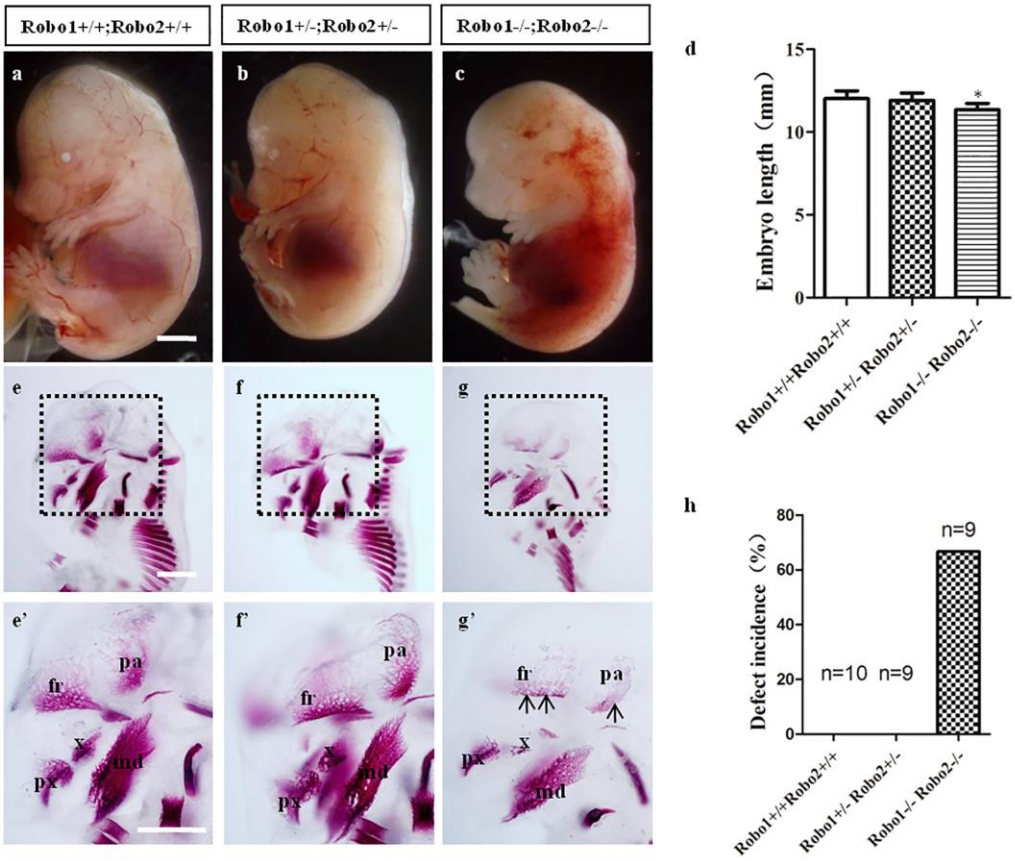

Figure 1 The deficiency of Robo1 gene caused the defect of cranial osteogenesis of mouse embryos

a-c: The representative 15.5-day mouse images from Robo1$^{+/+}$Robo2$^{+/+}$ (a), Robo1$^{+/-}$Robo2$^{+/-}$ (b) and Robo1$^{-/-}$Robo2$^{-/-}$ (c) mouse group respectively (n≥4). **d**: The bar chart showing the comparison of mouse length among Robo1$^{+/+}$Robo2$^{+/+}$, Robo1$^{+/-}$Robo2$^{+/-}$ and Robo1$^{-/-}$Robo2$^{-/-}$ mouse groups. **e-g**: Alizarin Red S staining was performed in A-C mouse embryos. Representative images of upper part of mouse body from Robo1$^{+/+}$Robo2$^{+/+}$ (e), Robo1$^{+/-}$Robo2$^{+/-}$ (f) and Robo1$^{-/-}$Robo2$^{-/-}$ (g) mouse group respectively. **e'-g'**: High magnification images from the sites indicated by black dotted squares in E-G respectively. **h**: Bar chart showing the comparison of the incidence of pa, fr, md, x and px developmental defects among Robo1$^{+/+}$Robo2$^{+/+}$, Robo1$^{+/-}$Robo2$^{+/-}$ and Robo1$^{-/-}$Robo2$^{-/-}$ mouse groups. Abbreviations: pa, parietal bone; fr, frontal bone; md, mandible; x, maxilla; px, premaxilla. Scale bars =1mm in a-c, 1mm in e-g, and 1mm in e'-g'. Data are represented as mean±s.e.m. (n≥4). *P<0.05.

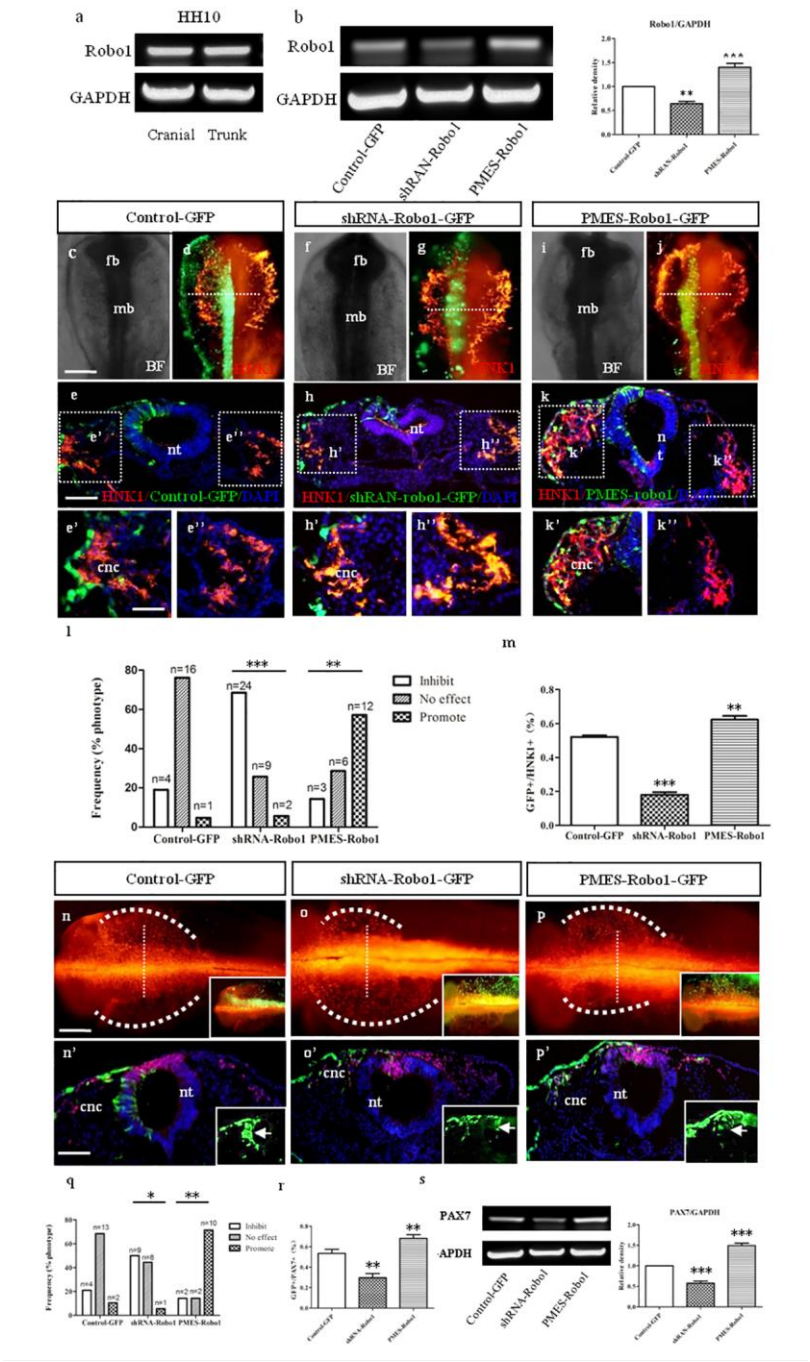

Figure 2 The up- or down-regulation of Robo1 gene expression affected the production of HNK1$^+$ and PAX7$^+$ chick cranial neural crest cells

Half-sides of HH3 chick embryos were transfected with the plasmids of Control-GFP (control), shRNA-Robo1-GFP (knock-down) and PMES-Robo1-GFP (over-expression), and the whole-mount fluorescent staining against HNK1 and PAX7 were performed after incubation for 30 hours. **a:** RT-PCR results revealed Robo1 expression in cranial and trunk portions of HH10 chick embryos. **b:** RT-PCR results

revealed Robo1 expression down-regulated or over-expressed in chick neural tube following shRNA-Robo1 and PMES-Robo1 transfection. The bar chart showing the ratio of shRNA-Robo1 and PMES-Robo1 expression to GAPDH in control and transfected embryos from RT-PCR data. **c-d**: Representative bright-field (c) and merge fluorescent images (d, GFP: green, HNK1: red) of chick embryo head transfected with Control-GFP. **e**: Transverse sections at the level indicated by dotted line in d. **e'-e"**: High magnification images from the sites indicated by black dotted squares in e respectively. **f-g**: Representative bright-field (f) and merge fluorescent images (g, shRNA-Robo1-GFP: green, HNK1: red) of chick embryo head transfected with shRNA-Robo1-GFP. **h**: Transverse sections at the level indicated by dotted line in g. **h'-h"**: High magnification images from the sites indicated by black dotted squares in h respectively. **i-j**: Representative bright-field (i) and merge fluorescent images (j, PMES-Robo1-GFP: green, HNK1: red) of chick embryo head transfected with PMES-Robo1. **k**: Transverse sections at the level indicated by dotted line in j. **k'-k"**: High magnification images from the sites indicated by black dotted squares in k respectively. **l**: Bar chart showing the comparison of phenotype numbers (inhibited, unchanged and elevated production of HNK1 positive cranial crest cells) among control, shRNA-Robo1 and PMES-Robo1 transfected embryos. **m**: Bar chart showing the ratios of GFP^+ cell and $HNK1^+$ cell number in the transverses sections of control, shRNA-Robo1 and PMES-Robo1 transfected embryos. **n-p**: Chick embryo head transfected with Control-GFP (n), shRNA-Robo1-GFP (o) and PMES-Robo1 (p). **n'-p'**: Transverse sections at the levels indicated by white dotted lines in n, o and p. PAX7 labeled neural crest cells from Control-GFP (n'), shRNA-Robo1-GFP (o') and PMES-Robo1 (p'). DAPI staining was performed for each section. The solid line square showing the transverse section from the embryo that was transfected with Control-GFP, shRNA-Robo1-GFP or PMES-Robo1 in neural tube. The arrows show the transfected side in the neural tube. **q**: Bar chart showing the number of experimental embryos and phenotype numbers (inhibited, unchanged and elevated production of PAX7 positive cranial crest cells) among control, shRNA-Robo1 and PMES-Robo1 transfected embryos. **r**: The bar chart showing the ratio of GFP^+ cell

numbers and total PAX7^{+} neural crest cell numbers among control, shRNA-Robo1 and PMES-Robo1 transfected embryos. **s**: RT-PCR results revealed PAX7 expression down-regulated and over-expression in chick neural tube following shRNA-Robo1-GFP and PMES-Robo1 transfection. The bar chart showing the ratio of Pax7 expression to GAPDH in control and transfected embryos from RT-PCR data. Abbreviations: fb, forebrain; mb, midbrain; BF, bright-field; nt, neural tube; cnc, crest neural cell. Scale bars =500 um in c-d, f-g, i-j, n-p; 40 um in e, h, k; 20um in e'-e", h'-h", k'-k", 30um in n'-p'. Data are represented as mean±s.e.m. (n≥4). *P<0.05, **P<0.01 and ***P<0.001.

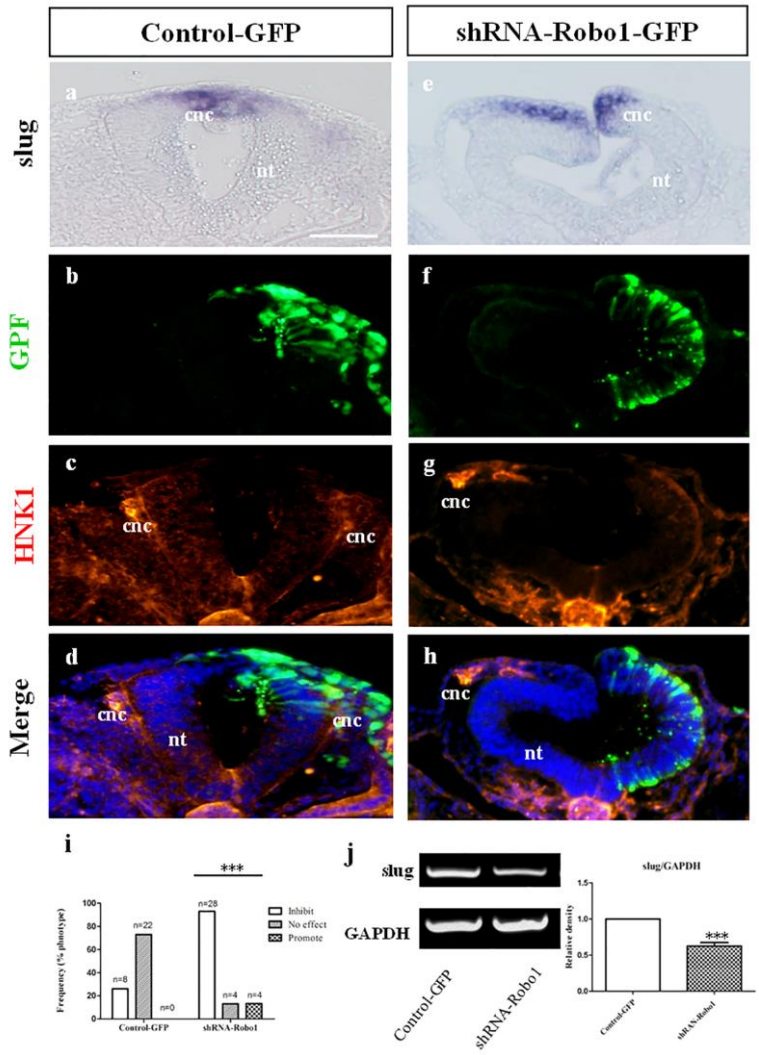

Figure 3 Down-regulating Robo1 gene level restricted slug expression in cranial neural crest cells

Half-side neural tubes of HH3 chick embryos were transfected with the plasmids

of shRNA-Robo1-GFP (knock-down) and Control-GFP. **a-d**: Slug *in situ* hybridization and HNK1 immunofluorescent staining were performed in Control-GFP transfected chick embryos. **e-h**: Slug *in situ* hybridization and HNK1 immunofluorescent staining were performed in shRNA-Robo1-GFP transfected chick embryos. a, e Slug *in situ* hybridization in head region. b, f Image of Control-GFP and shRNA-Robo1-GFP transfected embryo. c, g Image HNK1 immunofluorescent staining one. d, h Merged image of DAPI, image b, f and c, g. **i**: Bar chart showing the number of experimental embryo and phenotype numbers (inhibited, unchanged and elevated production of slug^{+} cranial crest cells) among control and shRNA-Robo1 transfected embryos. **j**: RT-PCR results revealed slug expression down-regulated in chick neural tube following shRNA-Robo1-GFP transfection. The bar chart showing the ratio of slug expression to GAPDH in control and transfected embryos from RT-PCR data. Abbreviations: nt, neural tube; cnc, crest neural cell. Scale bars = 30um in a-h. (n≥4). ***P<0.001.

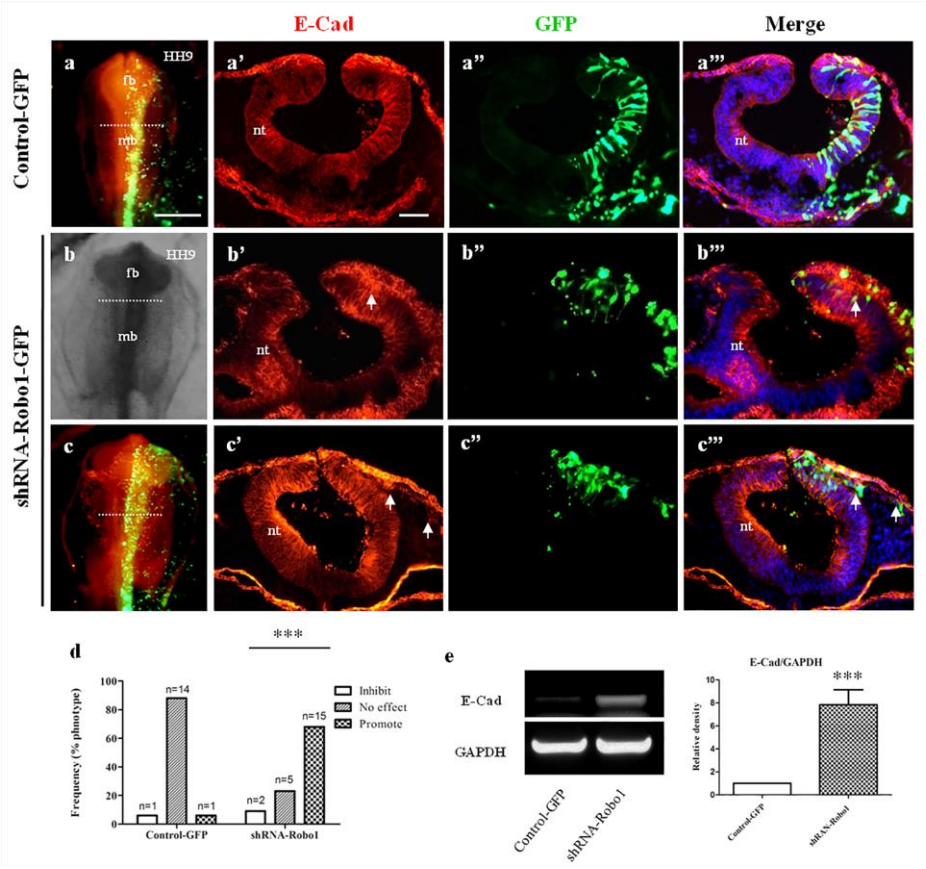

Figure 4 Down-regulating Robo1 gene level promoted E-Cadherin expression in early chick embryos

a: Fluorescent images for E-Cadherin expression (red) and Control-GFP (green) transfection in chick embryonic head. **b-c**: Representative bright-field image (b) and fluorescent images for E-Cadherin expression (red) and shRNA-Robo1-GFP (green) transfection (c) in chick embryonic head. **a'-a''', b'-b''' and c'-c''':** Transverse sections at the levels indicated by white dotted lines in a, b and c respectively showing E-Cadherin expression (a'-c'), Control-GFP and shRNA-Robo1-GFP transfected (a''-c'') and merged (a'''-c''') in chick embryonic head. The arrows point to examples of co-localization of GFP and E-Cadherin cells (a'''-c'''). **d**: Bar chart showing the number of experimental embryo and E-Cadherin promote expressed numbers among control and shRNA-Robo1 transfected embryos. **e**: RT-PCR results showing E-Cadherin expression in chick neural tube following shRNA-Robo1-GFP transfection. The bar chart showing the ratio of E-Cadherin expression to GAPDH in control and transfected embryos from RT-PCR data. Abbreviations: fb, forebrain; mb, midbrain; nt, neural tube. Scale bars = 500 um in a-c, 30 um in a'-a''', b'-b''' and c'-c'''. (n≥4). ***P<0.001.

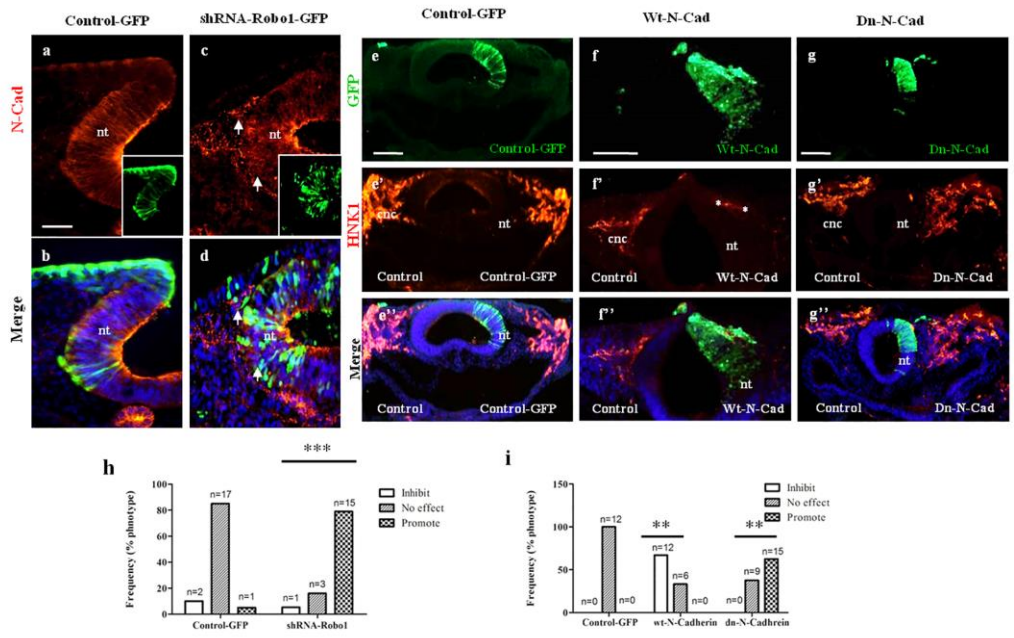

Figure 5 Down-regulating Robo1 gene level also elevated N-Cadherin expression in developing neural tube

a-b: Transverse sections of Control-GFP transfection showing the N-Cadherin

expression (a) and the combination with DAPI staining and GFP (b). The solid line square showing the transverse section from the embryo that was transfected with Control-GFP in half of neural tube (a). **c-d**: Transverse sections showing shRNA-Robo1 transfection (c), the N-Cadherin expression (c) and the merged image with DAPI (d) half-side neural tube. The solid line square showing the transverse section from the embryo that was transfected with shRNA-Robo1-GFP in half of neural tube (c). The arrows point to the examples of co-localization of GFP and N-Cadherin cells (c-d). **h**: Bar chart showing the number of experimental embryo and N-Cadherin promote expressed numbers among control and shRNA-Robo1 transfected embryos. **e**: Transverse section from the embryo that was transfected with Control-GFP in half-side neural tube. **e'-e"**: e' HNK1 immunofluorescent staining (red) was performed in the same transverse sections in e. e" merged image of e , e' and DAPI. **f**: Transverse section from the embryo that was transfected with Wt-N-Cad-GFP in half-side neural tube. **f'-f"**: f' HNK1 immunofluorescent staining (red) was performed in the same transverse sections in f. f" is the merge image of f, f' and DAPI. **g**: Transverse section from the embryo that was transfected with Dn-N-Cad-GFP in half-side neural tube. **g'-g"**: g' HNK1 immunofluorescent staining (red) was performed in the same transverse sections in g. g" is the merge image of g, g'and DAPI. **i**: Bar chart showing the number of experimental embryo and phenotype numbers (inhibited, unchanged and elevated production of $HNK1^{+}$ cranial neural crest cells) among control and either Wt-N-Cad or Dn-N-Cad transfected embryos. Abbreviations: N-Cad, N-Cadherin; Wt-N-Cad, wild type N-Cadherin; Dn-N-Cad, dominant negative N-Cadherin; nt, neural tube; cnc, cranial neural crest. Scale bars =20 um in a-d, 20 um in e-g and 20um in e'-e'', f'-f'' and g'-g''. ($n \geqslant 4$). **P<0.01, ***P<0.001.

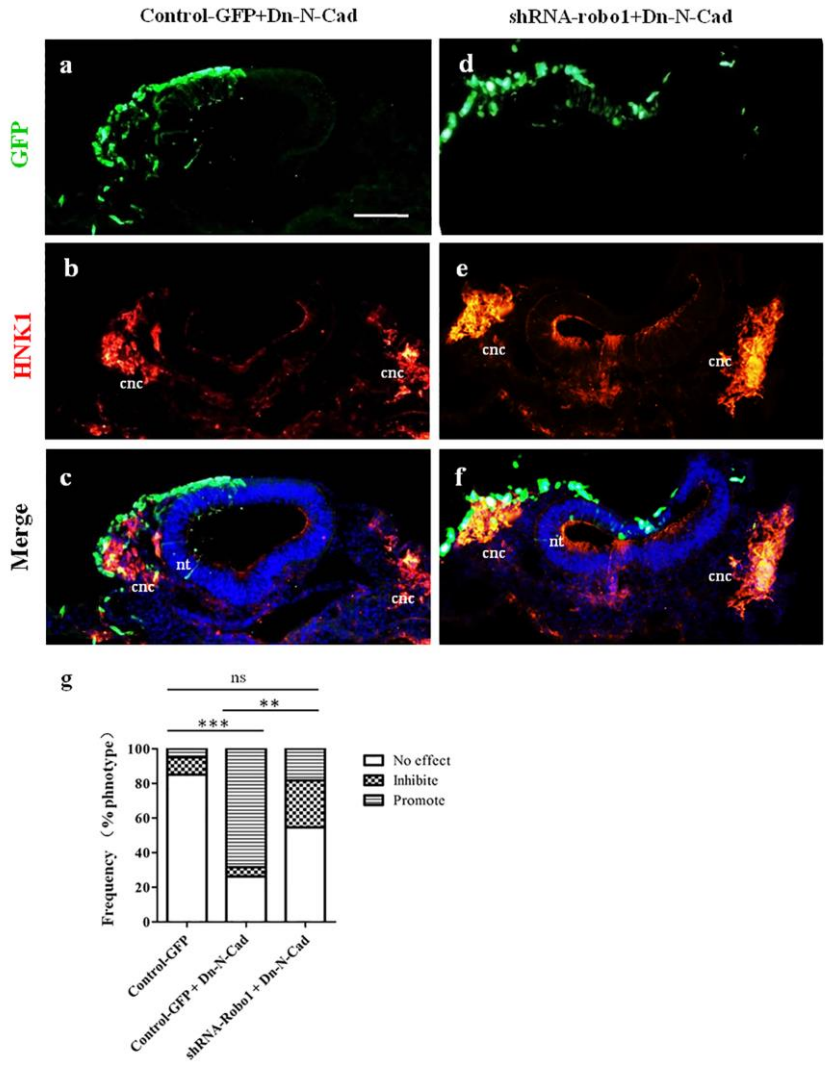

Figure 6 Simultaneously knocking down robo1 and N-Cadherin did not affect cranial neural crest cell production in chick embryos

a-c: Transverse sections showing the co-transfection of Control-GFP and dn-N-Cadherin representive GFP image (a), HNK1 immunofluorescent staining image (b), and the merge images of a-b and DAPI staining (c). **d-f:** Transverse sections showing the co-transfection of shRNA-Robo1-GFP and dn-N-Cadherin representive GFP image (d), HNK1 immunofluorescent staining (e) and merged image of d-e and DAPI staining (f). **g**: Bar chart showing the percent of the number of experimental embryo and phenotype numbers (inhibited, unchanged and elevated production of HNK1+ cranial neural crest cells) among the transfection of Control-GFP, the co-transfection of Control-GFP and dn-N-Cadherin, the co-transfection of shRNA-Robo1-GFP and dn-N-Cadherin transfected embryos. Abbreviations: nt,

neural tube; cnc, crest neural cell. Scale bars = 30 um in a-f. (n≥6). **P<0.01

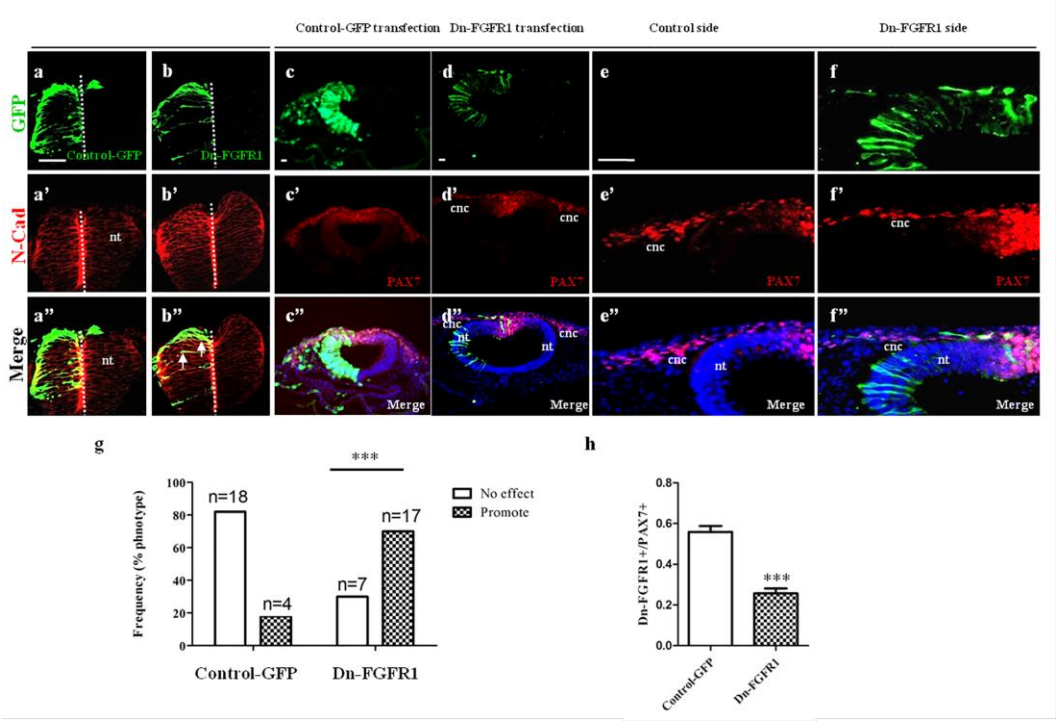

Figure 7 Down-regulating FGFR1 did not affect the expression of N-Cadherin in chick embryos and down-regulating FGFR1 restricted the production of PAX7^{+} cranial neural crest cells

a-b: Half-side neural tubes were transfected with either Control-GFP (a, control) or Dn-FGFR1 (b). **a'-b'**: N-cadherin immunofluorescent staining was performed in the same transverse sections in a and b respectively. **a"-b"**: Merged images of a-b and a'-b' respectively. The arrows indicate the examples of co-localization of GFP and N-Cadherin positive cells (b''). c-c'': Half-side neural tubes were transfected with Control-GFP (c), PAX7 immunofluorescent staining image (c'), and merged images of c-c' and DAPI staining (c''). d-d'': Half-side neural tubes were transfected with Dn-FGFR1 (d), PAX7 immunofluorescent staining image (d'), and merged images of d-d' and DAPI staining (d''). **e-f**: Transverse sections showing the control-side neural tube (e) and Dn-FGFR1 transfected side (f) in the neural tube. **e'-f'**: Pax7 immunofluorescent staining was performed in the same transverse sections in e and f respectively. **e"-f"**: Merged images of e-f and e'-f', and DAPI stained in each sections. **g**: Bar chart showing the phenotype frequency (inhibited or unchanged production of N-Cadherin^{+} cranial neural crest cells) among control and Dn-FGFR1

transfected embryos. **h**: Bar chart showing the ratio of GFP^+ cell numbers and total $PAX7^+$ neural crest cell numbers among control, Dn-FGFR1-GFP transfected embryos. Abbreviations: N-Cad, N-Cadherin; Dn-FGFR1, dominant negative FGFR1; cnc, cranial neural crest; ps, primitive streak; nt, neural tube. Scale bars = 20 um in a-a'', b-b'', c-c'', d-d'', e-e'' and f-f''. Data are represented as mean±s.e.m. (n≥4), ***P<0.001.

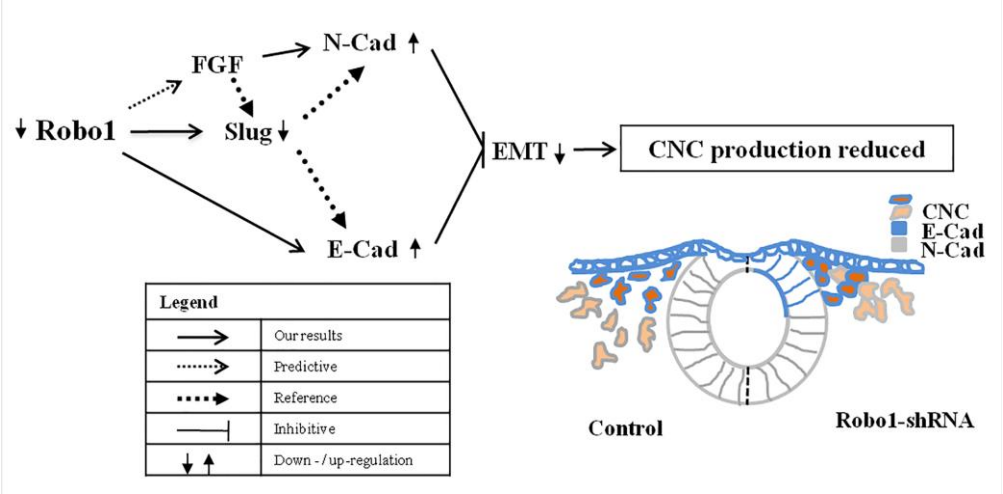

Figure 8 A proposed model that depicts the potential mechanisms for how knocking-down Robo1 reduced production of cranial neural crest cells